Electromagnetic design of a high frequency PM machine for the propulsion of a hybrid sportscar

by

Brackovic Damir

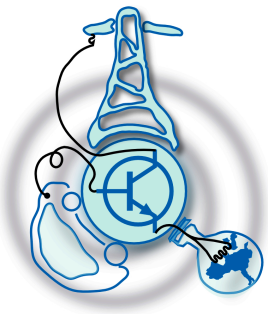

Submitted to the Department of Electrical Engineering, Electronics, Computers and Systems
in partial fulfillment of the requirements for the degree of

Erasmus Mundus Master Course in Sustainable Transportation and Electrical Power Systems

at the

UNIVERSIDAD DE OVIEDO

September 2015

Author .....

Certified by .....
Fabio Giulii Capponi
Assistant Professor
Thesis Supervisor

Electromagnetic design of a high frequency PM machine for the propulsion of a hybrid sportscar

by

Brackovic Damir

Submitted to the Department of Electrical Engineering, Electronics, Computers and Systems
on September 10, 2015, in partial fulfillment of the
requirements for the degree of
Erasmus Mundus Master Course in Sustainable Transportation and Electrical Power Systems

Abstract

The thesis deals with the initial design of a high-performance PM machine which is intended to serve as a shaft-mounted, integrated starter-generator (ISG) of a hybrid sportscar. Strict limitations on machine dimensions and performance (high overload torque, high operating frequencies) have been imposed making the design a challenging process. Final design has to result in an extremely linear machine in order to achieve required torque levels, but in the same time capable of field weakening (FW) over very wide speed range. Finite element analysis (FEA) is used as a tool in electromagnetic and thermal design stages. Torque behavior and reduction of machine losses are in the focus of electromagnetic design. Thermal analysis is performed once the geometry and materials choice have been finalysed in order to estimate temperature rise and heat flow in various machine parts.

Thesis Supervisor: Fabio Giulii Capponi
Title: Assistant Professor

Acknowledgments

First and foremost, I would like to thank my supervisor, Prof. Giulii Capponi, for his guidance, patience and support in the process of completing this Master Thesis. I would also like to thank professor Giulio De Donato, for his valuable assistance throughout my work on this project.

Finally, I wish to thank my family for uncoditional love and support during my Master's programme.

Contents

List of Figures

List of Tables

Introduction

This thesis deals with the design of a PM machine which is intended to serve as a shaft-mounted, integrated starter/generator (ISG) of an internal combustion engine (ICE) for a hybrid sportscar. Considering the application, strict limitations on machine dimensions and performance (high starting torque, wide constant power speed ratio) have been imposed making the design a challenging process. Final design has to result in an extremely linear machine in order to achieve required torque levels, but in the same time capable of field weakening (FW) over very wide speed range.

Several machine types suitable for ISG application are briefly discussed pointing out main advantages and disadvantages of each type. A geometry which is capable of meeting the requirements is presented afterwards.

FEA software (Infolytica's MagNet®) is used to model the machine geometry in two dimensions and to perform electromagnetic analysis. Series of static and dynamic, parametric 2-D simulations are performed in order to try to maximize torque production and estimate main machine constants. Flux density levels in PMs are observed in operating conditions to inspect the possible irreversible demagnetization. Several different materials (high quality steels) suitable for stator implementation in a high performance machine are considered and compared in terms of torque behaviour and total losses. Copper losses are displayed for the full operating speed range. As a method of reduction of these losses, increasing the number of turns inside slots with appropriate connections is tested. Infolytica's ThermNet® software is used once the geometry and materials have been selected. 2-D static FEA needs to be performed in order to inspect the temperature rise and heat flow in different machine components.

Objectives of the MTh

The objective of this Master Thesis work is to perform preliminary electromagnetic and thermal design analysis of an electric machine which will be used as an integrated starter/alternator in a hybrid sportscar. Torque behaviour, materials selection, losses analysis, temperature rise and heat flow need to be inspected performing two-dimensional finite element analysis (2-D FEA) to check if the design is able to meet the requirements.

Application requirements

A direct-drive integrated starter/generator machine is to be designed to complement the internal combustion engine of a hybrid sportscar. ISG has to be located on the crank shaft between ICE and the gearbox which means severe requirements in machine dimensions are imposed. Main constraints and performance requirements are listed below:

- maximum axial lenght 6 centimeters;
- maximum diameter 230 milimeters;
- starting torque of 350 Nm for a 3 seconds period;
- generating mode up to 10000 rpm;
- peak power of 15 kW(maximum 10 seconds);
- continuous power of 8 kW;

- generating power at 700 rpm $\geq$ 3kW

Achieving such high value of starting torque is a complex task and final design has to result in an extremely linear machine in order to meet this requirement. As a generator, machine needs to operate at very high frequencies which requires effective field weakening (FW) over a very wide speed range. For a machine to be able to achieve effective FW a high value of inductance is required which is contradictory to the first requirement of having an extremely linear behaviour.

State of the Art

Pyrhönen et. al. (2008) deal with the design process of rotating machines in general - basic principles, dimensioning, magnetic circuit analysis, resistances, flux leakages, insulation, heat transfer etc. Gieras (2010) focuses on the design process of permanent magnet (PM) machines and gives an insight in final element analysis (FEA) theory. Bianchi et. al. (2012) explain the procedure for electromagnetic and thermal analysis of an interior PM machine in a FEA software. Pre-processing stages (i.e. meshing, boundary conditions assignment) are thoroughly described and FEA results are displayed and discussed (i.e. torque behaviour, steady-state temperature rises).

Hybrid electric vehicles (HEVs) today represent an alternative to traditional internal combustion engine (ICE) vehicles. Much attention is given to improving the fuel efficiency and reducing the emissions of these type of vehicles. Viorel et. al. (2004) explain how the implementation of an integrated starter/generator (ISG) machine benefits the efficiency and performance of HEVs. Two main configurations (belt-driven and shaft-mounted machines) are discussed and compared.

Machine types including induction machines, switched-reluctance machines, permanent magnet machines have been considered for ISG application. Ferraro et. al. (2006), Carrichi et. al. (2001) explain why permanent magnet machines, in compact axial-flux topology (AFPM), are considered as most suitable machine type for an integrated starter/generator.

A slotted, single-stator, double-rotor AFPM machine is adopted for the ISG application described in this work. Slots are filled with flat conductors used to form the winding in order to achieve a very high fill factor. Slots are closed with soft magnetic composite (SMC) wedges. De Donato et. al. (2010, 2012, 2013) display positive

effects of SMC wedges - torque maximization and loss reduction among other.

Chapter 1

Integrated Starter/Generator

1.1 Introduction

In automotive industry, single electric machine capable of replacing the conventional starting motor and generator is called the integrated starter/generator (ISG). Hybrid electric vehicles (HEVs) equipped with this type of machine along with a conventional internal combustion engine (ICE) are often referred to as "mild" hybrid electric vehicles. Compared to "full" hybrids, power ratings of electric machines and battery sizes in "mild" hybrids are significantly lower which reduces the overall weight and cost of the vehicle. Compared to conventional (ICE) vehicles, benefits in improved electricity generation, ICE efficiency and fuel economy are present. Elimination of starter motor which is a passive component during ICE operation and coupling system between generator and crank shaft are important benefits of "mild" HEV powertrain.

Two common types of ISG configurations are belt-driven machine and direct-drive machine placed on the crankshaft between ICE and gearbox. Due to the complexity in construction and general higher cost of belt-driven configuration, direct-drive machine is a favoured ISG variant.

Acting as a starter motor, ISG is able to start ICE faster than conventional starter motors. In this "engine cranking" mode, high starting torque is required (for short time periods) which greatly exceeds torque levels necessary in generating mode. For generator operation, field weakening in very wide speed range is desired which makes

the design process of this machine extremely challenging due to contrary requirements.

Integrated starter/generator also provides power assistance to the ICE at low speeds or under high accelerations when extra power is required.

1.2 Machine type selection for ISG application

Variety of electric machines can be considered for ISG application. Key features that are required are high starting torque and wide constant power speed range (CPSR). Excellent mechanical strength of machine components (rotor especially) is required in a direct-drive ISG configuration due to the high rotating speeds. Research has been done on induction machines (IM), switched reluctance machines (SRM) and synchronous machines with permanent magnets (PMSM). Induction machines present a low cost, robust solution but thermal issues, small air gaps, narrow CSPR are some of the encountering issues. Switched reluctance machines have good CPSR but overcoming high torque ripple which these machines display is a challenging task. PMSM are an attractive option due to availability of high performance magnets, along with simpler and less expensive construction, high torque density and high efficiency. Interior permanent magnet machines (IPM) are capable of achieving wide CPSR due to the saliency, but mechanical strength of rotor structure is questionable. Risk of demagnetization is also high because of ineffective cooling arrangements of permanent magnets. Surface-mounted permanent magnet machines (SPM) offer better mechanical strength of rotor structures and better cooling arrangements but do not offer wide CPSR. Table 1.1 displays a brief comparison between these machine types with highlighted advantages and challenges for the ISG application [5].

Machine type	*Advantage*	*Challenge*
IM	robust construction low cost	thermal issues starting torque small airgaps complex control
SRM	robust construction high saliency-wide CPSR	torque ripple audible noise complex rotor design
IPM	cheaper converter solid rotor	rotor mechanical strength thermal issues (demagnetization)
SPM	mechanical strength ventilation	costly converter limited CPSR

Table 1.1: Machine type comparison for ISG application

As can be seen from the table, trade-offs have to be made when selecting the machine type since there is no ideal solution. Factors which will, in the end, be decisive in the selection process are machine desired performance, dimensions and the cost.

Considering the severe geometrical restrictions and performance requirements (high-performance, direct-drive ISG), a promising configuration has proven to be axial-flux permanent magnet (AFPM) double rotor, single stator (torus-type) configuration. Machine stator is iron core, slotted with ring-type, core-wound windings[3]. Ring-type windings are non-overlapping and have an advantage in relatively short axially directed end turns which results in reduced power loss and machine efficiency increase. Two externally placed rotors have surface-mounted magnets which are placed in "NN" configuration (opposite magnet poles are of the same polarity). Main parts and layout of this type of AFPM machine are shown in the figure 1-1.

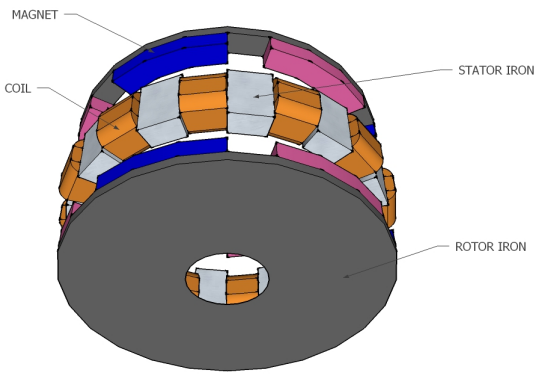

Figure 1-1: AFPM machine with 2 external rotors and ring-type windings

Geometry presentation

Table 1.2 lists the main machine parameters chosen for the specified application.

Parameter	*Dimension*
Stator outer diameter	200 (mm)
Stator inner diameter	120 (mm)
Slot height	12.2 (mm)
Slot width	6 (mm)
Stator yoke thickness	10.6 (mm)
Rotor yoke thickness	5 (mm)
PM thickness	6 (mm)
Air gap length	2 (mm)
Phase number	3
Pole number	14
Max. operating frequency	1166.67 (Hz)
Number of slots	42
Number of slots per pole per phase (Q)	1
Fill factor (k_{fill})	0.7

Table 1.2: Machine parameters

By using flat, rectangle shaped conductors it is possible to achieve a high fill factor (k_{fill}=0.7). Stator slots are partially closed with magnetic wedges. Compared to open slots, magnetic wedges offer multiple advantages: assistance in torque maximization, total loss reduction and avoiding PM demagnetization among other [6],[7],[8].

Materials assigned to the initial model are listed in the table 1.3.

Component	*Material*
Stator	Non-oriented electrical steel M250-35A
Rotor	Pure iron ARMCO
PM	NdFeB - VACODYM677HR®
Conductors	Copper
Wedges	Soft magnetic composite Somaloy 500

Table 1.3: Materials used for 2-D FEA

The chosen geometry is displayed in the figure 1-2.

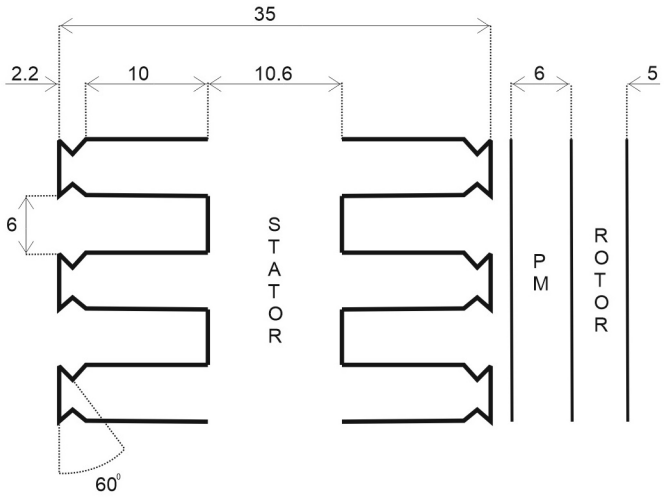

Figure 1-2: Main machine dimensions

1.2.1 Permanent magnet material

In commercial production today, the most important permanent magnet materials are:

- Ferrites;
- Somarium-cobalt (SmCo);
- Neodymium-iron-boron (NdFeB).

Ferrites appeared in the 1950s and are most dominant type of permanent magnets in the market due to their low price. Another important advantage over two other groups is their ability to withstand high operating temperatures. Ferrites display the lowest remanence (B_{rem}) and coercivity (H_c) which makes them unsuitable for implementation in high performance machines like the one described in this work. Remanence (remanent magnetic flux density) is the magnetic flux density corresponding to zero magnetic field intensity. Coercivity represents the magnetic field intensity which corresponds to zero flux density - demagnetizing field value. Both, remanence (B_{rem}) and coercivity (H_c) decrease with the increase in PM temperature[12].

SmCo magnets are characterized with good heat resistance (operation up to 250°C) and good corrosion resistance. High price is their main disadvantage.

The most suitable PM type for implementation in high performance machines are NdFeB rare-earth magnets. Invented in 1983, these materials typically include 65% iron, 33%neodymium, 1.2% boron and small amounts of aluminium and niobium[15]. They exhibit the highest remanence and coercivity, high energy density and with addition of other rare-earth elements they are able to sustain temperatures up to 190°C.

Table 1.4 displays the main properties of different permanent magnet materials (adapted from[1]).

Curie temperature is the point at which the material experiences the change in magnetic properties - permanent magnetism changes to induced magnetism. T_{max} is the maximum operating temperature.

Property	*Ferrite*	*SmCo*	*NdFeB*
B_{rem}(T)	0.38	0.85	1.15
H_c(kA/m)	250	570	880
Curie T(°C)	450	775	310
T_{max}(°C)	300	250	180
density(kg/m^3)	4800	8300	7450
$\Delta B_{rem}/\Delta T$(%/°C)	-0.20	-0.04	-0.12
$\Delta H_{ci}/\Delta T$(%/°C)	0.40	-0.2	-0.7

Table 1.4: Main properties of hard magnetic material

For this application NdFeB VACODYM677HR® from Vacuumschmelze was choosen with the main properties displayed in the table 1.5.

Property	*VACODYM 677 HR*
B_{rem}(T)	1.18
H_c(kA/m)	915
Curie T(°C)	310-370
T_{max}(°C)	190
density(kg/m^3)	7700
$\Delta B_{rem}/\Delta T$(%/°C)	-0.095
$\Delta H_{ci}/\Delta T$(%/°C)	-0.5

Table 1.5: Main properties of VACODYM 677 HR

Chapter 2

Electromagnetic Design of the ISG Machine - Torque Analysis

2.1 Introduction

In this chapter main concepts of electromagnetic design using finite element analysis (FEA) are demonstrated in order to roughly predict and adjust the machine behaviour to desired performance requirements. Two-dimensional model of the machine is presented and pre-processing stages of FEA are explained (e.g. meshing, boundary conditions). High quality permanent magnet material choosen for the application is tested to assess the possible risk of irreversible demagnetization. Torque analysis has been carried out and parameters like synchronous inductance and phase resistance are estimated. Electromagnetic analysis of the ISG machine has been carried out with the help of finite element analysis in MagNet® software from Infolytica.

FEA is a numerical, iterative technique for solving partial differential equations as well as integral equations. It offers approximate results which are sufficient in analysis of complex structures like electrical machines. This work deals with the initial design stage of the machine and for that purpose 2-D FEA analysis has been carried out in order to save time and computing resources (compared to 3-D analysis).

FEA of an electric machine in MagNet® consists of three main parts: pre-processing, solving and post-processing. Pre-processing part includes constructing

the machine geometry, assigning the materials, boundary conditions, creating the mesh and setting the simulation properties. MATLAB® is used for this stage where a script has been writen to construct the model geometry, set solving parameters and set the link to MagNet® software. Solving process is performed by the software according to parameters specified by the user. Two solving methods are available - Newton-Raphson and Successive Substitution method (3-D only). User also specifies the solving accuracy - Newton tolerance and Conjugate Gradient (CG) tolerance. Newton tolerance is used to linearize the system of equations in an iteration loop. The CG tolerance is used to determine when the iterative solution algorithm has converged to the solution of the linearized matrix system resulting from the discretization of the model[14]. Post-processing stage includes extraction and interpretation of the results displayed in the Global Results Window of the software.

2.2 Modelling the machine geometry in 2-D

In order to construct the machine model in two dimensions, rotational motion of the two rotors is replaced with translational motion. Cylindrical section of the machine at the average radius (80 mm, figure 2-1) is developed over a plane. Due to the symmetry in machine geometry (both electromagnetic and geometric), it is possible to "cut" the machine along the stator yoke in circumferential direction and to present only one rotor and half of the stator yoke as the model for FEA. Boundary conditions allow for further simplification - studying just one pole of the machine. This fraction of the complete machine si enough to perform FEA and to save significant time and computing memory resources compared to constructing the full model. Figure 2-2 shows the MagNet® environment where one pole pitch is modeled for the 2-D analysis.

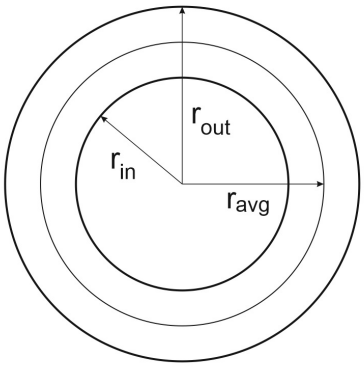

Figure 2-1: Average radius used to represent 2-D machine model

Planar symmetry has been assumed so that the magnetic field has the same value in each section of the machine in z-axis direction. Air gap is divided into four layers of the same thickness. Multiple air gap layers are required in order to properly model the large field gradients that might occur. Air gap layers next to the stator and rotor are assigned with 'Virtual Air' material while two inner layers are assigned with 'Air' material. "Virtual Air has the same properties as Air and is used in order to improve the accuracy of force and torque calculation" [14].

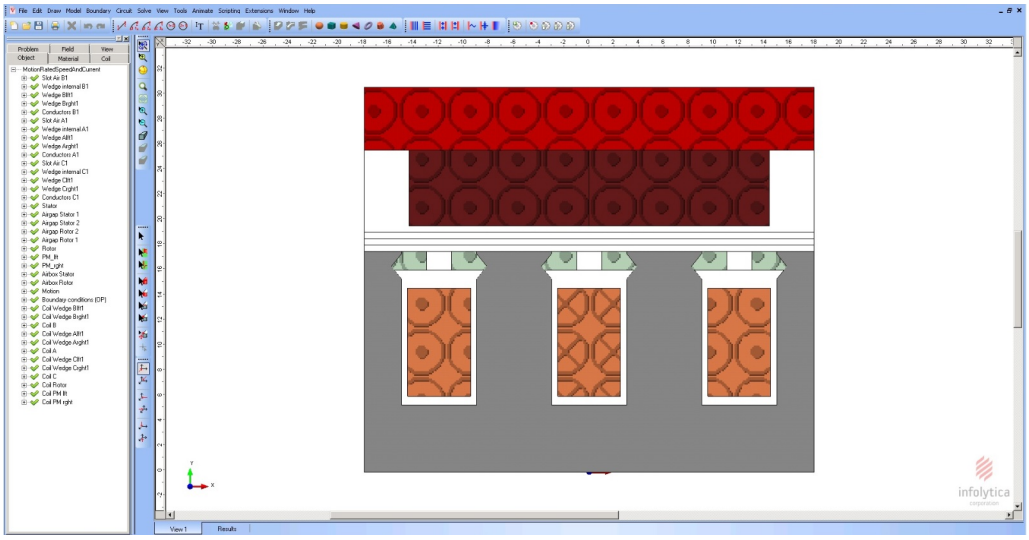

Figure 2-2: MagNet® environment and geometry constructed for FEA analysis

Wedges, magnets and stator yoke, together with conductors, are defined as coils in order to inspect the losses appearing in these components.

2.3 Meshing

For obtaining correct and valid results in FEA, meshing process has to be performed with caution. Model is divided into a mesh of elements (triangles in 2-D analysis) and the field solution is calculated in the triangle nodes (represented by a polynomial with unknown coefficients). The smaller the mesh size is, the more accurate the solution is because errors in geometrical modeling are reduced and the fields' variations are represented more accurately. However, very small mesh elements can significantly increase the computational time without significant increase in the solution accuracy. For that reason, it is important to reduce mesh size (or increase the polynomial order, or both) in areas where the direction or magnitude of the field is changing rapidly (e.g. air gap). MagNet® software offers a feature to automatically adapt and refine mesh size which is used in this analysis. Initial maximum element size for the mesh generation (specified in pre-processing) is given in the table 2.1.

Air gap being the most sensitive part to large field variations, has the smallest mesh size in order to achieve more accurate results.

Component	*Maximum element size (mm)*
Conductor	0.25
Slot air	0.25
PM	0.5
Wedges	0.25
Airgap	0.125
Stator	1
Rotor	1

Table 2.1: Maximum element size for meshing procedure

Initial mesh of the model is shown in the figure 2-3. Solution mesh slightly differs from the initial mesh in the air gap area since the improving mesh quality feature is enabled (self-adaptive meshing).

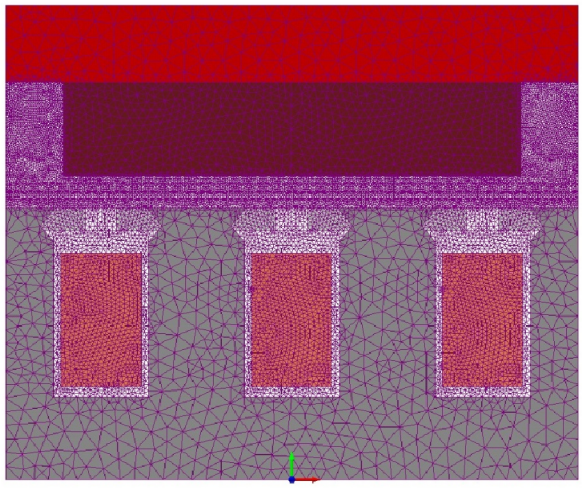

Figure 2-3: Initial mesh generation

2.4 Boundary conditions

Boundary conditions are used to specify the behaviour of the unknown fields on the outer surfaces of the model [14]. An Air Box (artificial outer boundary) is constructed to limit the extent of the computational domain and boundary conditions are applied

to Air Box surfaces. In this case, Air Box encompasses the model edges.

Generally, in a magnetic field problem, four main boundary conditions exist [1]:
Dirichlet boundary condition: specifies a known value of the magnetic vector potential A = const (typically A = 0) along a line or a surface, for example on the outer surface of the machine which means that field lines are parallel to this boundary.
Neumann boundary condition: forces the flux density lines to be normal to a selected surface or line (e.g. infinite permeability iron).
Periodic boundary condition: imposes the same magnetic vector potential behaviour along the lines or surfaces.
Anti-periodic boundary condition: imposes that the magnetic vector potential behaviour is opposite from line to line(surface to surface).

Boundary conditions in MagNet® are listed as:
- unary (field behavior is specified on a given surface) - flux tangential, field normal, surface impedance, thin plate;
- binary (a relation between two surfaces is specified) - even, odd periodic.

In the model described in this work, odd periodic boundary condition has been imposed on the geometry presented in the figure 2-2. In the pre-processing stage (in the MATLAB® script), surfaces (or faces in MagNet®) have been selected and assigned with odd periodic boundary conditions (fig 2-4, represented with'+ -' symbols). This boundary condition is used due to the machine periodicity property (its properties are repeating periodically).

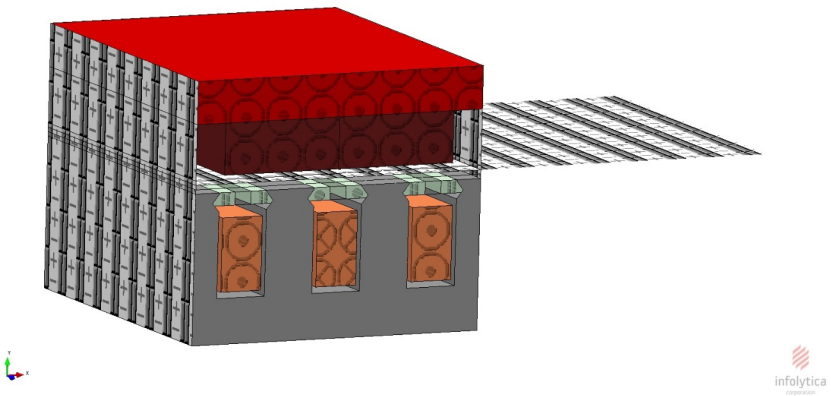

Figure 2-4: Odd periodic boundary conditions assigned, 3-D representation

2.5 Field maps

In the post-processing stage it is possible to display different field quantities using field maps e.g. flux density levels reached in certain machine parts as well as to visualize and show flux lines and their distribution in the machine. These maps are given in x-y plane and all quantities that can be visualized have only x component and y component (e.g. $\mathbf{H}=(H_x, H_y, 0)$). This feature is useful since iron saturation can be observed, leakage and fringe flux lines can be visualized giving an insight in field solution and model behaviour.

Figure 2-5 shows the flux density distribution and flux lines produced just from permanent magnet - no stator currents are flowing. Here, we can see that all flux coming from the PM is aligned on the direct axis (cuts the magnet in half). Flux lines bypassing the required path that can be seen (at the sides of the magnet) represent leakage flux while the "bulged" lines at the PM edges represent fringing flux. Flux density along the air gap, established by the PM on the rotor, has the shape shown in the figure 2-6. Local minimums in this curve represent the effect of slot openings. Peak value of flux density along the air gap is taken as magnetic loading (B_m) of the machine.

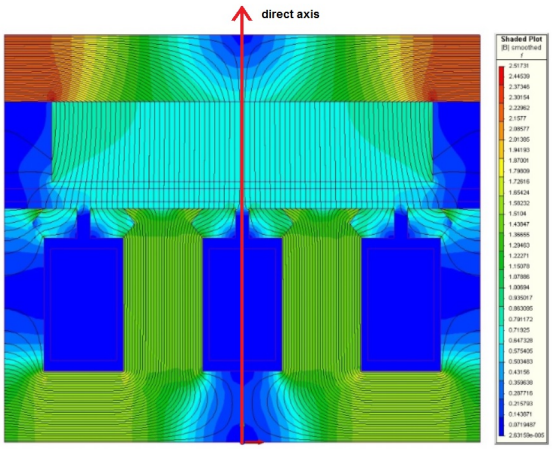

Figure 2-5: PM flux density distribution and flux lines

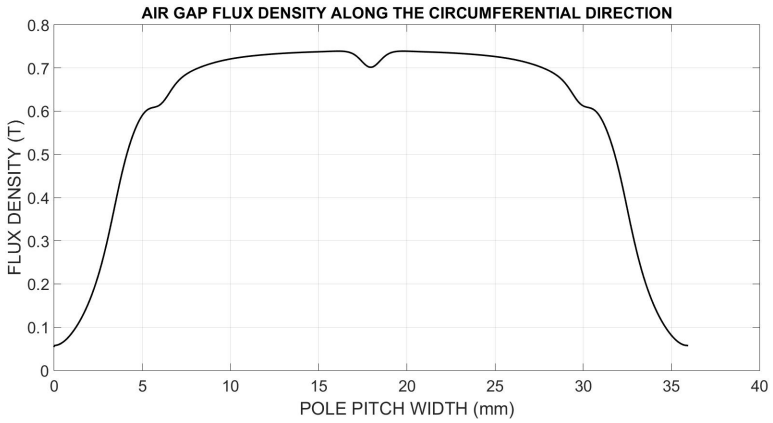

Figure 2-6: Flux density along the airgap

Figure 2-7 shows the field lines and flux density distribution created just by phase currents - when no PM field is considered. In the position shown here phase A (middle coil) instantaneous current has a value of 472 (A), while currents for B and C phases have values of -236 (A)[1].

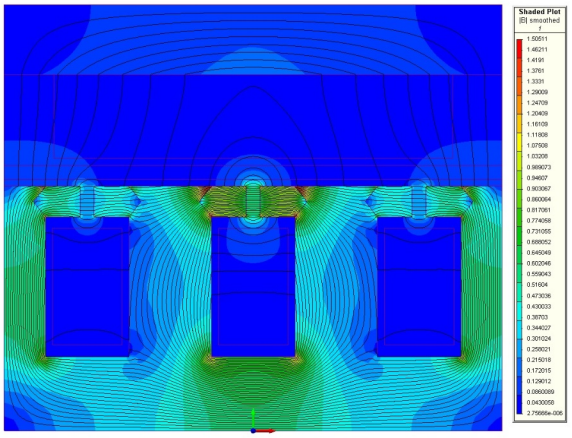

Figure 2-7: Flux density distribution and flux lines due to the phase currents

[1]Procedure for obtaining these currents is explained in the following section

2.6 Torque estimation

Following torque analysis has been carried out in the 'qd0' synchronous reference frame with rotational speed being synchronous speed and d-axis aligned with the PM flux rotating vector [4]. Torque eqation for a synchronous PM machine in synchronous reference frame is given in the following form:

$$T = \frac{3}{2} \cdot P \cdot (\lambda_d \cdot i_q - \lambda_q \cdot i_d) \tag{2.1}$$

$$\lambda_d = \lambda_{PM} + L_d \cdot i_d \tag{2.2}$$

$$\lambda_q = L_q \cdot i_q \tag{2.3}$$

where

- P is number of pole-pairs;
- λ_d, λ_q are direct and quadrature axis flux linkages;
- i_d,i_q are direct and quadrature axis currents;
- L_d,L_q are direct and quadrature axis inductances;
- λ_{PM} is PM flux linkage;

The torque equation becomes:

$$T = \frac{3}{2} \cdot P \cdot (\lambda_{PM} \cdot i_q + (L_d - L_q) \cdot i_d \cdot i_q) \tag{2.4}$$

First term in this equation is proportional to the PM torque and is called synchronous torque while the second term is called reluctance torque. Since the machine of interest is magnetically isotropic, surface-mounted PM machine, the reluctance torque component does not exist and the final torque equation is:

$$T = \frac{3}{2} \cdot P \cdot \lambda_{PM} \cdot i_q \tag{2.5}$$

2.6.1 Theoretical torque vs. current curve

The first step in torque analysis is to construct a theoretical torque versus current (T=T(i)) curve based on equation 2.5. In order to find the value of PM flux linkage(λ_{PM}) necessary for the calculation, a transient no-load simulation with motion has been performed. Two electrical periods have been simulated with the initial position shown in figure 2-2 and with the simulation step of 18 electrical degrees (20 steps per electric period). Figure 2-8 shows the result of FEA: extracted 3 phase flux linkages while figure 2-9 shows their corresponding direct axis and quadrature axis components.

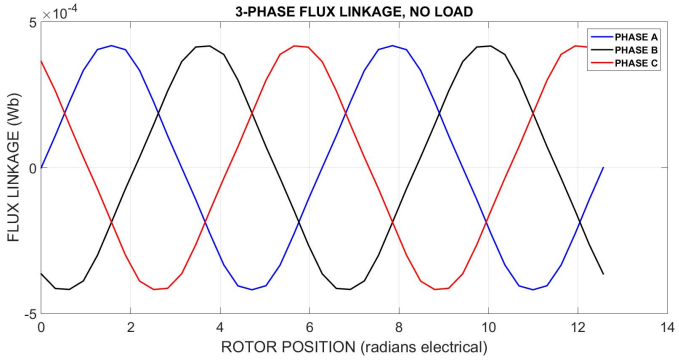

Figure 2-8: Flux linkages in coils - 3 phase components

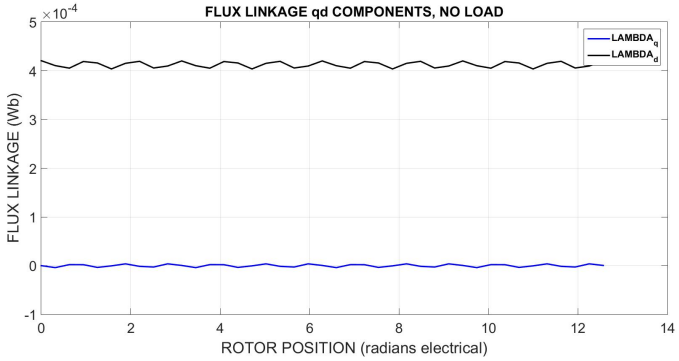

Figure 2-9: Flux linkages in coils - dq components

Transformation of the flux linkage values from the 3-phase sinusoidal to qd0 components is performed with the transformation matrix K:

$$K = \frac{2}{3} \cdot \begin{bmatrix} \cos(\theta) & \cos(\theta - \frac{2\pi}{3}) & \cos(\theta - \frac{4\pi}{3}) \\ \sin(\theta) & \sin(\theta - \frac{2\pi}{3}) & \sin(\theta - \frac{4\pi}{3}) \\ \frac{1}{2} & \frac{1}{2} & \frac{1}{2} \end{bmatrix}$$

$$\lambda_{qd0} = K \cdot \lambda_{abc} \tag{2.6}$$

As can be seen from the figure 2-9 the quadrature axis flux linkage is zero and flux is aligned on the direct axis only. The result presented is obtained just for one pole pitch in one half of the machine (fig 2-2) and to obtain the total value λ_{PMtot} for the whole machine, multiplication by 2 (because just one rotor is represented) and by number of poles is required:

$$\lambda_{PMtot} = \lambda_{PM} \cdot 14 \cdot 2 = 11.6(mWb) \tag{2.7}$$

After finding the value for PM flux linkage, we are able to construct the theoretical T(i) curve based on equation 2.5:

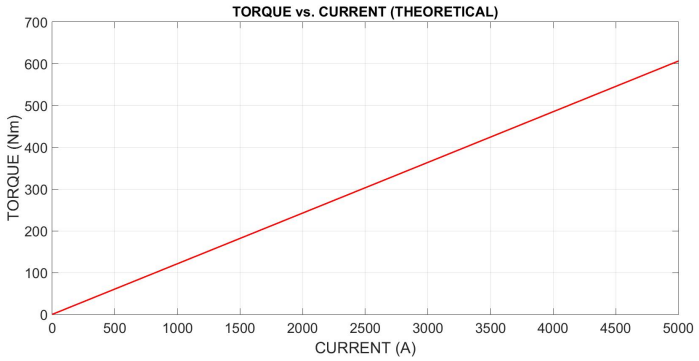

Figure 2-10: Theoretical torque vs. current curve

The curve in this graph is ideal, no saturation is present. It would be desirable for the design to have torque-current graph as close as possible to the ideal one presented here. In reality, machine will enter saturation with increasing current, and torque values will differ from these shown in theoretical, ideal curve.

Assuming the machine will be water-cooled, permissible value of continuous slot current has to be in the range of 300 (Arms) - $I_{cont} \sim 300$ A which results in continuous

torque value of around 50 (Nm) - $T_{cont} \sim 50$ Nm. Considering the requirement for continuous power of 8 (kW), nominal speed of 1530 (rpm) can be calculated:

$$\omega_n = \frac{P_{cont}}{T_{cont}} \cong 1530(rpm) \tag{2.8}$$

With the DC link of 48 (V) in the vehicle, limitation for the induced phase voltage (back EMF) is $E_{n,ph} \cong 16$ (V). Nominal value of phase current can be calculated from:

$$P_{cont} = 3 \cdot E_{n,ph} \cdot I_{n,ph} \tag{2.9}$$

$$I_{n,ph} \cong 167(Arms) \tag{2.10}$$

This current value can give us number of conductors per slot (N_c):

$$N_c = \frac{167}{300} = 1.8 \cong 2 \tag{2.11}$$

Nominal slot current equals to $I_{n,slot} = 334$ (Arms) or 472 (A) peak value. Finally, nominal values for speed and torque can be calculated as:

$$\omega_n = \frac{1.8}{2} \cdot 1530 \cong 1400(rpm); T_n \cong 56(Nm) \tag{2.12}$$

2.6.2 Torque vs. current curves from FEA

The ability to calculate force and torque is one of the most valuable features of FEA software. Four most important methods for torque calculation in FEA are:

- Maxwell stress tensor;
- Co-energy method;
- Lorentz force equation;
- Rate of change of energy field method.

The most frequently used method and the one used in MagNet® is Maxwell stress tensor method. After FEA solution is obtained, components of the force (in x,y and z directions) are presented in the Global Results Window. Torque is obtained by multiplying the force component in x-direction (circumferential direction) with the average radius:

$$T = F_x \cdot r_{avg} \tag{2.13}$$

where r_{avg} in this case is 80 (mm). Torque value obtained is valid just for one pole pitch and total torque value follows after multiplying with a factor of 28 (due to machine symmetry). In the pre-processing phase (MATLAB® script) the value for i_d current is set to zero - only operation with q-axis current is considered (no field weakening):

$$I = \sqrt{i_q^2 + i_d^2} = i_q \tag{2.14}$$

To obtain the T(i) graphs from the software, series of static 2-D simulations have been performed with q-axis peak current varying from 200 (A) to 6000 (A) with 200 (A) step. Simulation of "cold start" with PM temperature set at 20 (°C) along with PM temperature at 150 (°C) are shown in following figures.

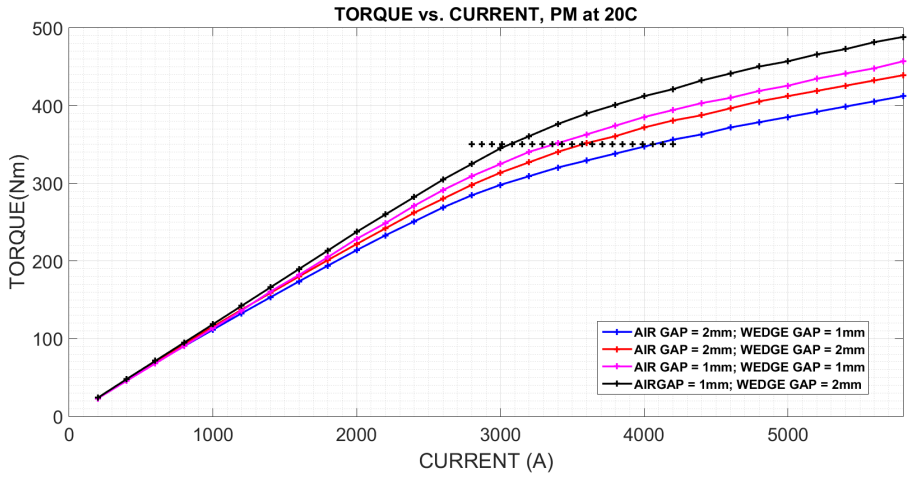

Figure 2-11: Torque vs. Current (Cold start, PM at 20 °C)

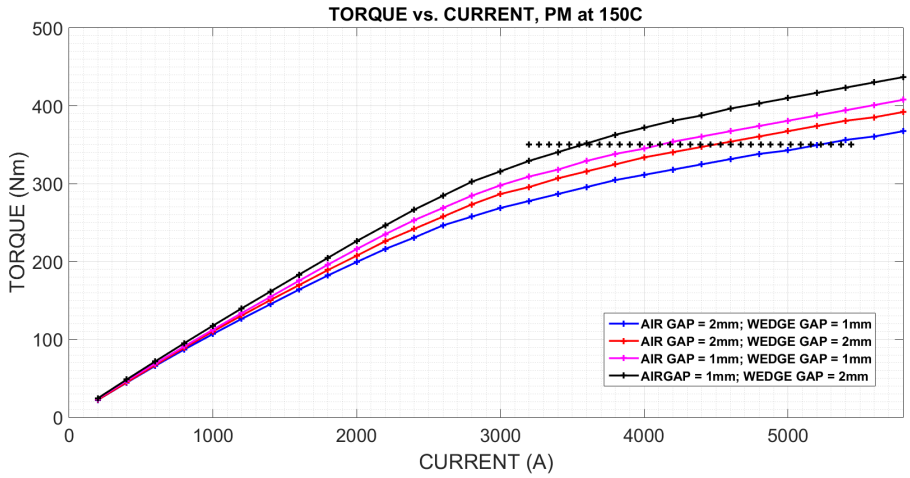

Figure 2-12: Torque vs. Current (PM at 150 °C)

Parametric analysis is also used where four combinations of air gap length and wedge gap length are considered. It is visible that combination of 1 (mm) air gap and 2 (mm) wedge gap offers highest value of torque for the injected current. During cold start (starter operation with PM temperature set at 20 °C) the machine is required to be extremely linear (to achieve 350 Nm torque level with very little machine saturation). This condition can be satisfied with the slot peak current having values in between 3000 (A) and 4000 (A). The combination of 2 (mm) air gap, 2 (mm) wedge gap geometry was adopted because the current necessary to achieve 350 (Nm) is in between of these two values.

Since the machine has to operate at very high frequencies, this relatively large air gap helps in keeping the magnet temperature low enough (lower losses in PM material due to the harmonic content in the air gap). Together with thick magnets, large air gap causes the synchronous inductance to have a low value which helps in torque maximization[15]. It is worth noting that air gap is a flexible parameter in AFPM machine design. It is easily adjustable which is an advantage over conventional radial-flux machines.

Running the motion simulation it is possible to display no-load cogging torque and torque achieved with nominal current value. Cogging torque is a result of interaction between the PM flux and the stator geometry (stator slots) with zero stator currents. This ripple is mainly described by the coenergy variation[1]:

$$T_{cog} = \frac{\delta W_{mc}}{\delta \theta_m} \tag{2.15}$$

where δW_{mc} is the magnetic coenergy and θ_m is the rotor position (mechanical angle).

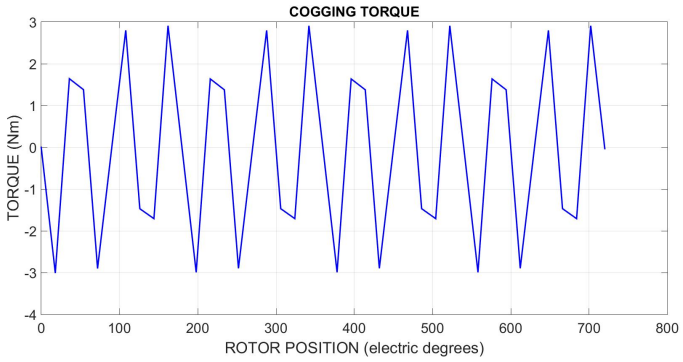

Figure 2-13: Cogging torque

Torque behaviour versus rotor position (electrical degrees) achieved with the q-axis peak current value of 472 (A) is shown in the figure 2-14 as a result of FEA (Maxwell stress tensor method).

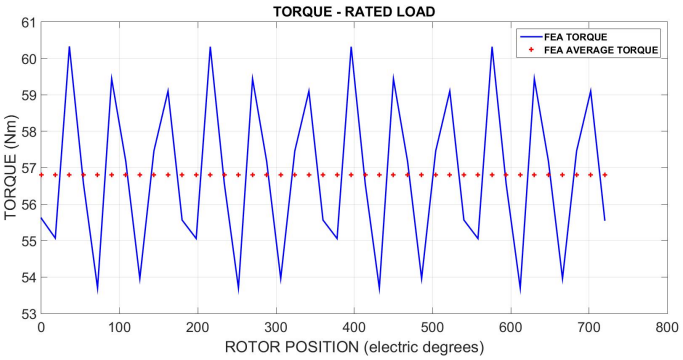

Figure 2-14: Rated torque value

From the FEA, average torque value is 56.8 (Nm). This value is very close to the value calculated with the equation 2.5 where obtained result for the q-axis current value of 472 (A) is 57.3 (Nm).

2.7 Induced voltage

In the Global Results Window (post-processing stage) induced voltages in the phase windings are calculated. No-load induced voltages in the coils (back EMF), under constant mechanical speed (ω_m=1400 rpm) condition are shown in the following figure:

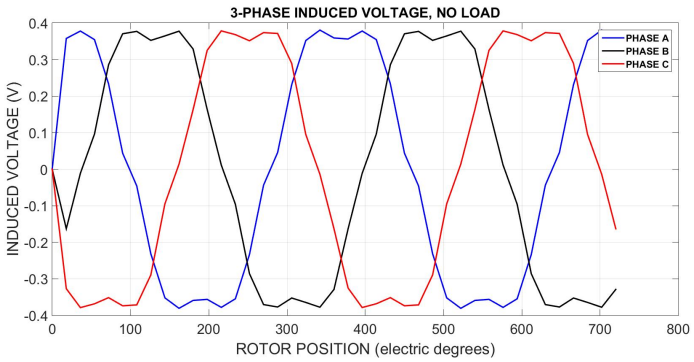

Figure 2-15: No load induced voltage

Relation to flux linkage (at no-load, shown in figure 2-8) is given with:

$$e(t) = \frac{d\lambda_t}{dt} \tag{2.16}$$

After scaling the obtained results (multiplying with the number of poles and with 2 due to half machine modeled) the value of induced voltage is:

$$E_{0,ph,rms}=7.536 \text{ (V)}.$$

With two conductors per slot, connected in series, this voltage approaches the allowed value of 16 (V). Under rated load condition (472 A peak) the induced voltage has the waveform displayed in figure 2-16.

The value of induced voltage is:

$$E_{ph,rms}=8.199 \text{ (V)}.$$

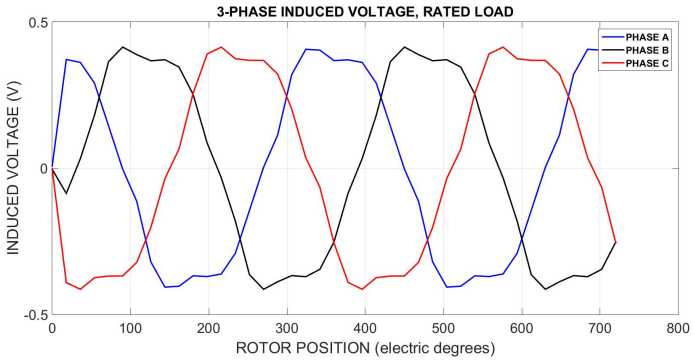

Figure 2-16: Induced voltage in the rated load condition

2.8 Synchronous inductance

Equation 2.3 can be used to estimate the value of synchronous inductance. Since the machine is surface-mounted PM machine, it is assumed that $L_d = L_q$. Transient simulation with rated current value (i_q=472 A peak value) has been performed and values for λ_q and λ_d have been obtained like in no-load case analyzed before.

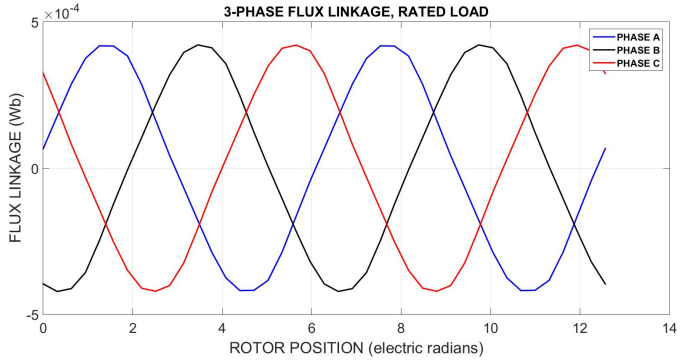

Figure 2-17: 3-phase flux linkage in coils

From the equation 2.3 we find:

$$L_q = \frac{\lambda_q}{i_q} = 4.24(\mu H)^2 \tag{2.17}$$

It is important however to notice that actual value of synchronous inductance will

[2]The model symmetry has been taken int the account - multiplication with pole number and second half of the machine

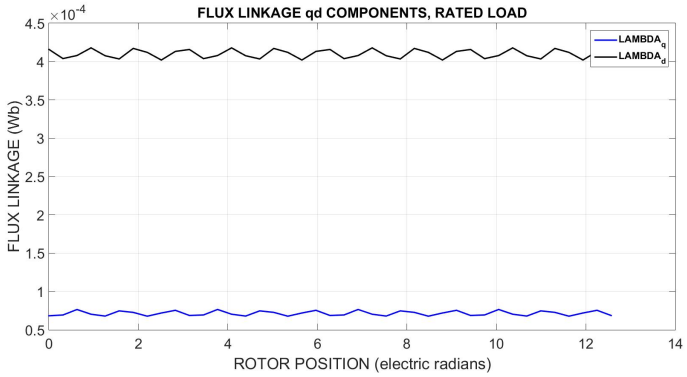

Figure 2-18: Flux linkage in coils - dq components

be different since this model does not include end-windings (end-windings inductance is neglected). To obtain more accurate prediction for this parameter, end-windings have to be modeled (3-D geometry) and 3-D FEA has to be performed.

2.8.1 Per unit value of synchronous inductance

With the value of induced voltage at rated load, it is possible to find per unit (p.u.) value of synchronous inductance ($l_{q,p.u.}$).

$$l_{q,p.u.} = \frac{L_q}{L_{base}} \tag{2.18}$$

Base value L_{base} is calculated with the base impedance (Z_{base}) and base speed (ω_{base}) with the following equation:

$$L_{base} = \frac{Z_{base}}{\omega_e} = \frac{E_{ph,rms}}{\omega_e \cdot I_{ph,rms}} \tag{2.19}$$

Per unit (p.u.) value $l_{q,p.u.}$ is:

$$l_{q,p.u.} = 17,73\% \tag{2.20}$$

Obtained result for per unit inductance is valuable because it is an indicator of how wide CPSR is achievable with controlling the stator currents. Consulting [2](graphs on pg. 5) it is obvious that desired CPSR cannot be achieved by controlling the stator currents. Unconventional methods of flux weakening (mechanical flux weakening), described in [10],[9], will be necessary to fulfill the requirements (not in the scope of this work).

2.9 PM demagnetization check

Using the FEA it is possible to check if permanent magnets are in risk of irreversible demagnetization during machine operation. Considering the desired machine requirements, PMs will be exposed to high temperatures and it is crucial to make a FEA simulation in MagNet® software where high temperatures are imposed on PMs.

While the machine is running, PMs are operating in the second quadrant of their magnetization (B-H) curve. The typical B-H curve and main properties for Neodymium-Iron-Boron PMs used in this analysis are given below (data taken from VACUUMSCHMELZE):

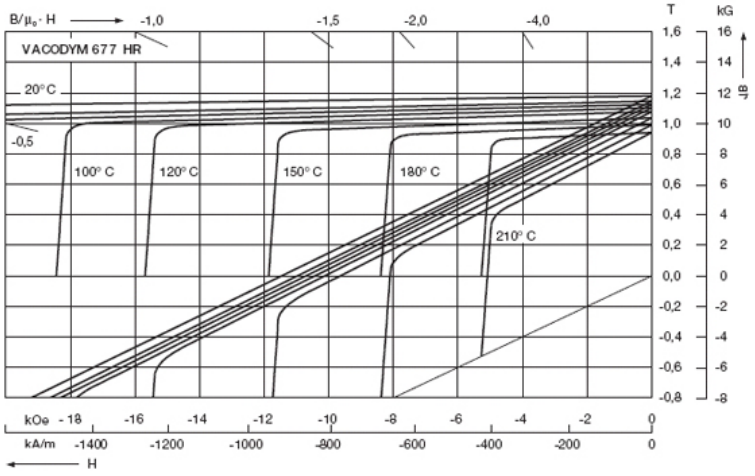

Figure 2-19: B-H curve for Vacodym 677 NeFeBr PM(vacuumschmelze.de)

In order for PMs to operate safely at high temperatures, minimum flux density should always be higher than flux density in the knee of curves shown in figure 2-19.

To perform demagnetization check, series of transient simulations were done with PM temperature set at two different values: 20(°C) and 150(°C). According to the information available from the PM manufacturer and the data provided in the software, the irreversible demagnetization occurs at flux density values reported in the table 2.2.

Starter operation was simulated - maximum starting torque at rotational speed of 400 (rpm). With PM temperature set at 20(°C) the critical value of flux density is -1.9 (T). Field maps were generated in the software post-processor and flux density

Temperature(°C)	*Demagnetization value of B(T)*
20	-1.9
60	-1.29
80	-1.01
100	-0.74
120	-0.489
150	-0.133
180	0.17
210	0.43

Table 2.2: Demagnetization values of flux density at different temperatures

(B_y component) is observed. Probe Field Values tool was used to read flux density values in different sections of the magnet during the rotor movement (two electrical periods were simulated). Field maps show that the lowest values of flux density in PM occur in the lower left corner (marked with red circle in the figure 2-20). The lowest measured value of flux density (B_y component) is around 0.3 (T) which can be considered safe for operation and far from the dangerous demagnetization value of -1.9 (T) at this PM temperature (20°C).

Afterwards, transient simulation with PM temperature set at 150(°C) was performed. Field inspection probe was used to check if the value of flux density (B_y) approaches the demagnetization value of -0.133 (T).

Results obtained from the cold start simulation with the PM temperature set at 20(°C) show that PM are not in danger of getting irreversibly demagnetized (figure 2-20). Even in harsh operating conditions, with PM temperature set at 150(°C), analysis shows that PM are still in the safe zone of B-H curve (flux density values remain positive throughout the motion simulation).

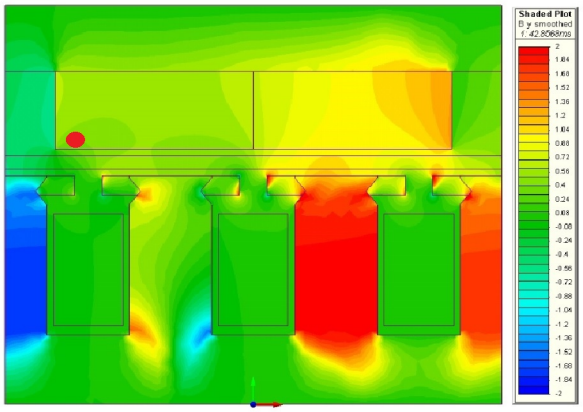

Figure 2-20: Field map, PM at 20°C, minimum flux density 0.3 (T)

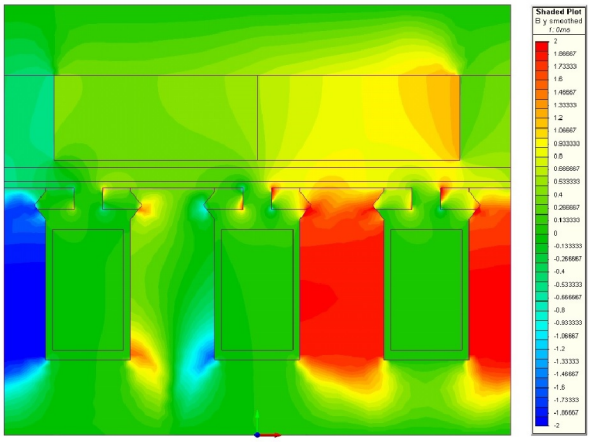

Figure 2-21: Field map, PM at 150°C, minimum flux density 0.14 (T)

Chapter 3

Electromagnetic Design of the ISG Machine - Losses Analysis

3.1 Introduction

Generally, machine losses can be divided into following categories[15]:

- Iron losses (core losses);
- Copper losses (resistive losses or Joule losses);
- Additional losses (electromagnetic losses not included in the resistive and iron losses);
- Mechanical losses;

In this part several different stator materials were compared and their impact on core losses and torque behaviour is displayed. Joule losses are calculated for the full speed range and the results are presented. Minimization of these losses is necessary and reduction is achieved with increasing the number of conductor turns and applying combination of series and parallel connection between the turns.

3.1.1 Iron losses

There are two types of iron losses in electric machines - hysteresis losses and eddy current losses. With the alternating current the core material's B-H curve is constantly circulated, resulting in hysteresis losses proportional to the operating frequency. With alternating flux being present in the core, voltages in the material are induced which cause the circulation of eddy currents. Negative effect of these currents is restricted by using thin laminations to form the stator core. According to [1], iron losses can be represented with following equation:

$$p_{iron} = k_{hy}\hat{B}^{\beta}f + k_{ec}\hat{B}^{2}f^{2} + k_{ex}\hat{B}^{\frac{3}{2}}f^{\frac{3}{2}} \tag{3.1}$$

where $\hat{B}$ is the peak of sinusoidally varying flux density at the frequency f, k_{hy} and k_{ec} are the hysteresis and the classical eddy current constants which can be supplied by the manufacturer. β is the Steinmetz constant often approximated as $\beta \simeq 2$. Constant k_{ex} is the eddy current excess losses constant[1]. From equation 3.1 it is visible that hysteresis losses are proportional to the operating frequency while eddy current losses are proportional to the square of operating frequency f.

3.1.2 Ohmic losses

Ohmic losses (losses in the copper, resistive losses or Joule losses) are formed in the machine windings. Generally, it is a parameter dependent on wire diameter and the total length of the conductors (including end-windings which are not taken into consideration in 2-D FEA). These losses are proportional to the square value of current and to the phase resistance:

$$P_{Cu} = mI^{2}R_{ph} \tag{3.2}$$

where m is the number of phases. Ohmic losses actually depend on the effective value of resistance under different operating conditions - different frequency and temperature. At high operating frequencies skin effect causes the current to flow through

outer, smaller cross-sectional area in conductor, which leads to the increase in the resistance value and in total ohmic losses (negative impact on machine efficiency). Ohmic losses can be separated in two components - frequency dependent (AC loss) component and frequency non-dependent (DC loss) component.

3.2 Stator material selection for the reduction of iron losses

The machine stator for this application is going to be constructed out of high quality, electrical, laminated steel. Those are specially processed steel alloys required to achieve excellent magnetic properties such as narrow hysteresis area (minimize the core losses) and high magnetic permeability across a wide range of frequencies. These materials are cut in thin sheets (less than 2 mm thick), thermally processed and stacked together to form the stator core. Non-oriented steel has to be used due to the presence of rotating parts (non-constant magnetic flux path).[1] The initial analysis was performed with stator material being non-oriented, fully annealed[2] electrical steel of M250-35A grade. This section shows the comparison of M250-35A material with five other non-oriented electrical steels with emphasis on T(i) curve and core losses. Materials considered for the possible stator implementation are listed in the table 3.1[3]:

Material Name	*Composition*
M250-35A	Silicon-Iron (SiFe), 0.35 mm
NO-12	Silicon-Iron (SiFe), 0.12 mm
NO-18	Silicon-Iron (SiFe), 0.18 mm
NO-20	Silicon-Iron (SiFe), 0.2 mm
VACOFLUX 48®	Cobalt-Iron (CoFe), 0.35 mm
VACOFLUX 50®	Cobalt-Iron (CoFe), 0.35 mm

Table 3.1: High quality steels considered for stator materials

[1] Non-oriented means there is no difference in the magnetic properties between the rolling direction and the transverse direction of the material - the material is isotropic.

[2] Thermally processed steel to remove stress from the machining process

[3] M250-35A and NO materials shown in the table are materials from Cogent Power Ltd.

First step is to check and update the material information in the software with the latest information provided by the steel manufacturers. Magnetic permeability of materials (B-H curves) as well as specific total loss at characteristic frequencies (W/kg) have been compared and if required, updated in the software.

Series of static simulations have been performed to find the current values necessary to obtain rated torque of 56 (Nm).
Rated values of slot currents (peak values) for considered stator materials are displayed below:

- M250-35A: 472 (A);
- NO materials(Cogent Power): 481 (A);
- VACOFLUX®materials: 415 (A);

The most important operating point that needs to be inspected is the maximum speed-rated torque point (10000 rpm; 56 Nm). This point has to be achieved using mechanical flux weakening in which the magnetic energy remains at the constant value and the flux linkage is reduced by means of mechanical displacement of two rotors[10]. In the software, parametric transient analysis is performed where core losses have been calculated for each considered stator material. Final results are obtained by summing the iron losses data from the Global Results Window in the software (time averaged hysteresis and eddy current loss) and multiplying them with a factor of 28 (due to symmetry). Results are displayed in the figure 3-1.

FEA results indicate that core losses for the reference material - M250-35A steel reach 1.2 (kW) at 10000 (rpm). This number is too high and other materials need to be considered. NO materials cause much lower core losses and the effect of steel sheet thickness can be clearly seen in figure 3-1. NO-18 steel (0.18 mm sheet thickness) at 10000 rpm has 10% lower iron losses than NO-20 while NO-12 (0.12 mm sheet thickness) steel has 28% lower losses compared to NO-20. However, materials which result in lowest core losses are VACOFLUX® materials (total core losses reduced ∼66% compared to M250-35A losses).

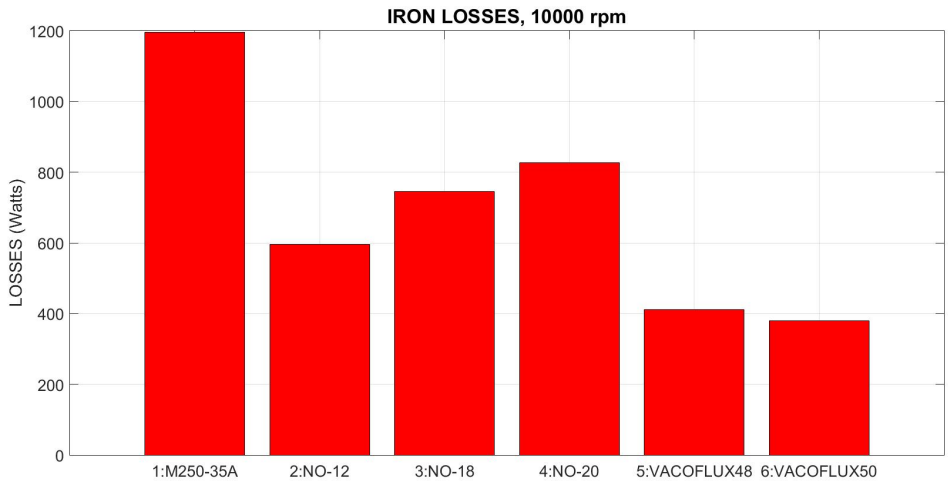

Figure 3-1: Iron loss for various stator materials, high speed operation

Figure 3-2 shows the iron losses at rated speed (1400 rpm) and rated torque (56 Nm) where VACOFLUX® materials produce the losses in the range ∼50% of the losses produced by M250-35A steel.

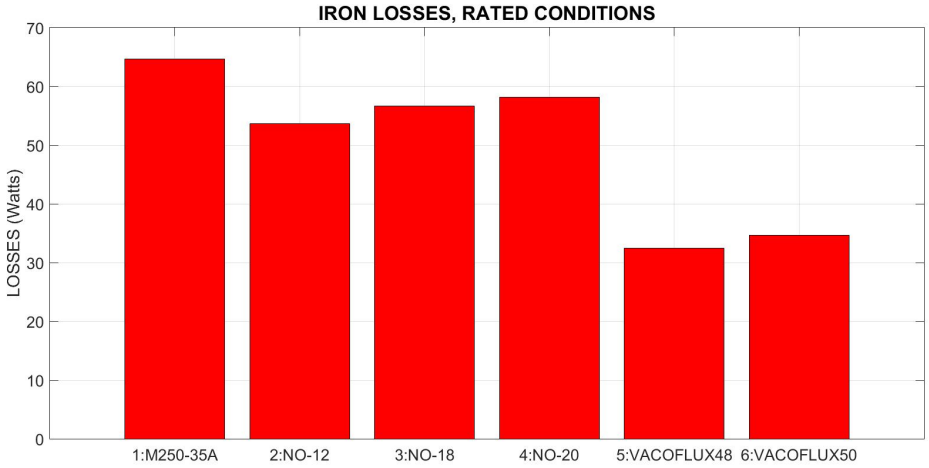

Figure 3-2: Iron loss for various stator materials, rated speed and torque

Based on the manufacturers data, curves representing specific losses at 50 Hz frequency, for analysed materials are shown in the figure 3-3.

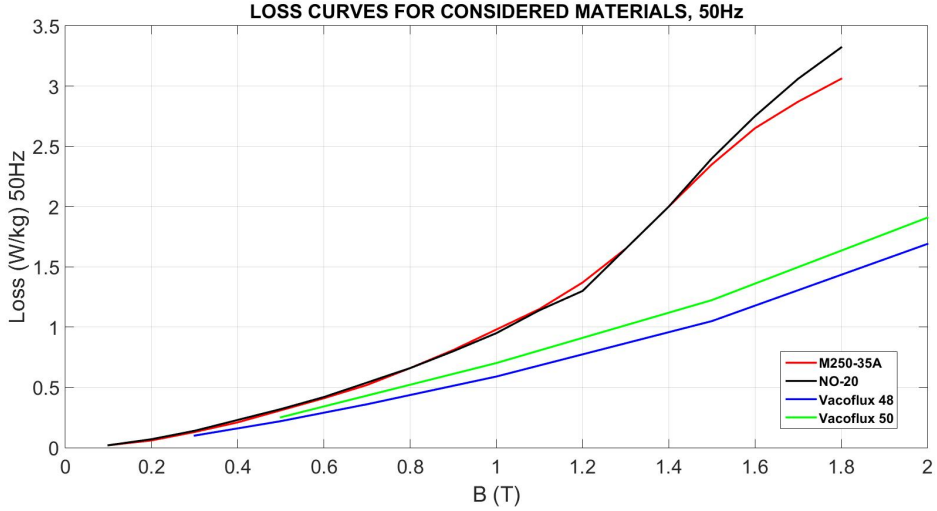

Figure 3-3: Specific losses at 50 Hz

Torque versus current graphs for cold start (PM temperature 20 °C) have been constructed again considering different stator materials. Phase current has been increased in 200 (A) steps from 200 (A) to 5800 (A) peak value. Results are displayed in the following figure:

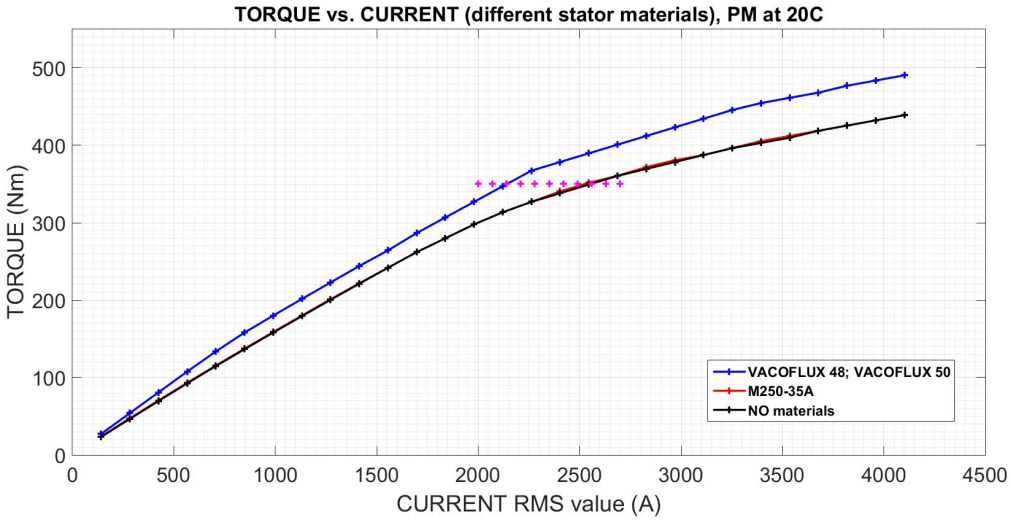

Figure 3-4: Torque vs. Current (different stator materials)

As can be seen from figure 3-4, machines with stator constructed from materials

M250-35A and NO display almost the same torque behaviour. However, machine with stator made out of one of VACOFLUX® materials achieves same torque levels with much lower slot currents compared to other materials. Desired maximum torque values are achieved without machine getting into saturation. This is very important feature of VACOFLUX® materials since lower current results in lower copper losses which is significant at higher operating frequencies.

The main reason for this superb behaviour is high value of saturation magnetization. For both analyzed VACOFLUX® materials saturation occurs at around 2.25 (T) while other tested materials saturate at around 1.8 (T)(figure 3-5).

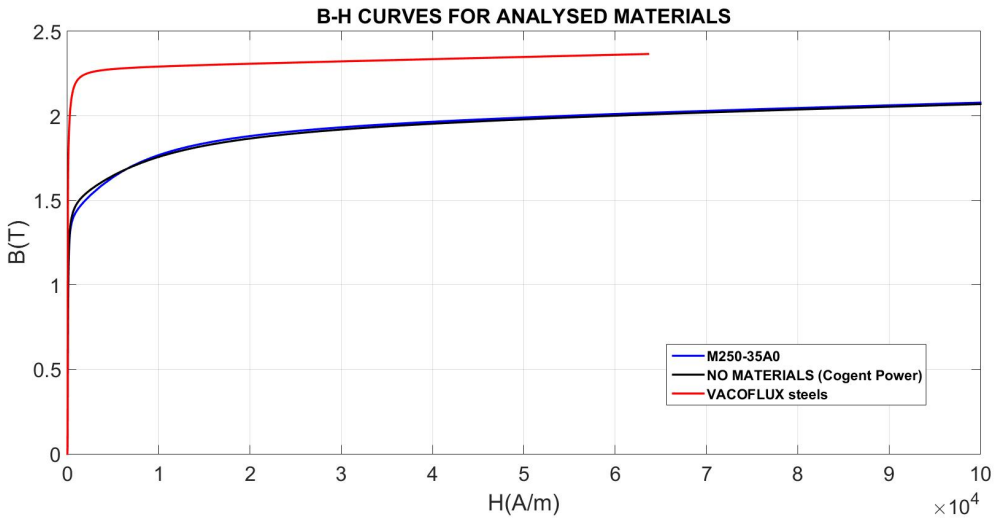

Figure 3-5: B-H curves of analyzed stator materials

Negative aspect of these materials can be considered their high price, availability on the market, and their density - 8.12 (g/cm^3) compared to 7.65 (g/cm^3) for NO materials and 7.6 (g/cm^3) for M250-35A steel.

3.3 Ohmic losses minimization

The analysis of ohmic losses in the software has been performed with stator material M250-35A and rated value of peak slot current: 472 (A). Since the modeled geometry is 2-D, losses in end-windings cannot be simulated. First simulation was carried out with geometry shown in figure 2-2. Here, only one conductor is placed in the slot forming the coil and is modeled as "stranded" in the pre-processing stage. When modeled like "stranded", only DC loss component can be obtained as a result since skin effect is not considered and uniform current density is imposed in conductors no matter of operating frequency. Results are acquired from the Global Results Window in the software (copper losses), summed together and multiplied by a factor of 28 (due to machine symmetry). The obtained result is $P_{DC} = 150.4$ Watts. With the help of equation 3.2 we can estimate the value of phase resistance (DC resistance):

$$R_{ph,DC} = \frac{P_{DC}}{3I_{rms}^2} = 0.45(m\Omega) \tag{3.3}$$

This value of phase resistance is not completely accurate since end-windings are not considered. However, obtained value can be improved with an approximation of the end-windings resistance. For this calculation, end-windings length is roughly estimated as a straight line (not an arc). DC resistance of the end winding is calculated as following:

$$R_{ew,DC} = \rho\frac{l_{ew}}{S} = 0.232(m\Omega) \tag{3.4}$$

where ρ is copper resistivity with value of $1.7331{\cdot}10^{-8}$ (Ωm), l_{ew} is the estimated end-winding length (41.2 mm in total for one full coil wound over stator yoke) and S is the copper area in the slot (43 mm^2). Adding this value to the DC phase resistance of copper active length we obtain:

$$R_{ph,DC} = 0.682(m\Omega) \tag{3.5}$$

The real value of phase resistance is not a constant value, it is frequency and temperature dependent.

Approximated total DC losses in end-windings are 77.6 (W) which consists to 51% of the DC copper losses inside the slots (active length of conductors). Naturally, conductors exhibit losses due to skin effect and proximity effect, which have significant values at higher operating frequencies. To simulate these losses, coils have to be modeled as "solid" instead of "stranded" in MagNet® software. This means that non-uniform current density profile is allowed according to Maxwell's laws. To maximize the machine efficiency, minimization of these losses has to be achieved. This can be done in several ways. In this work, increasing the number of conductors (two, four and eight conductors) connected in a certain way is attempted (to get more uniform current density distribution and to increase the skin depth). Another option of minimizing these frequency dependent losses is to use Litz wire instead of flat conductors. However, with using Litz wire it is not possible to achieve the same slot fill factor as when using flat conductors.

In the first stage, phase coils are modified so that existing conductor in the slot is replaced with with two turns(fig 3-6). The change in conductor thickness and series connection is done in the MATLAB® script by modifying the conductors geometry and assigning the appropriate current path in the coils.

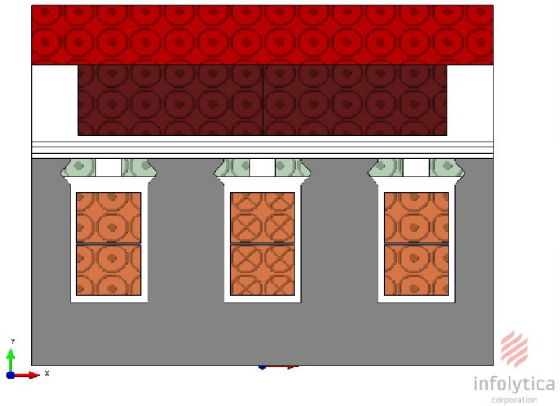

Figure 3-6: Two conductor turns per slot

As a result of this modification, half of the previous value of current can be injected in conductor (286 A instead of 472 A) in order to achieve the rated torque value of 56 (Nm) (N·i=const). As a consequence, this configuration also means that induced voltage is two times higher compared to initial analysis.

Further steps in reducing AC losses are replacing the two conductors per slot with four and eight conductors. In the case of four conductors forming the coil, two conductors on top are connected in parallel, then connected in series with two lower conductors, which are also connected in parallel.

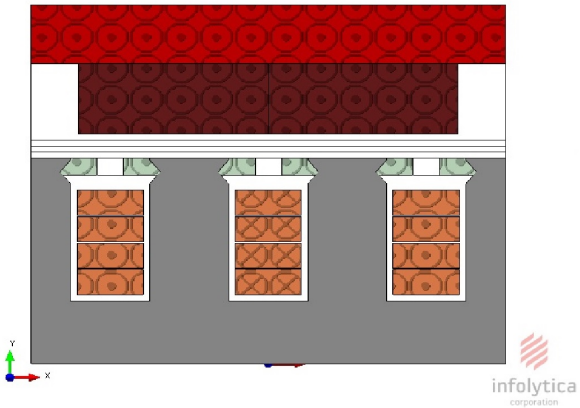

Figure 3-7: Four conductors per slot

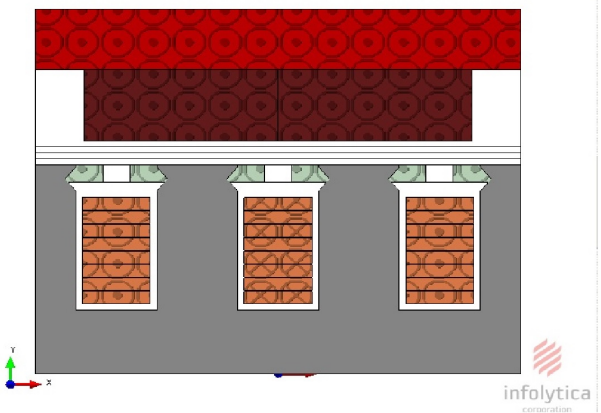

Figure 3-8: Eight conductors per slot

Parallel connection is done in order to reduce the negative influence of the skin effect when the machine is operating at high electric frequencies. Conductors in parallel connection display differences in induced voltages and in impedances which can result in circulating currents with negative effects such as the increase in conduction losses and forming of hot spots in the machine.

The comparison of copper losses for described modifications is shown in the figure 3-9.

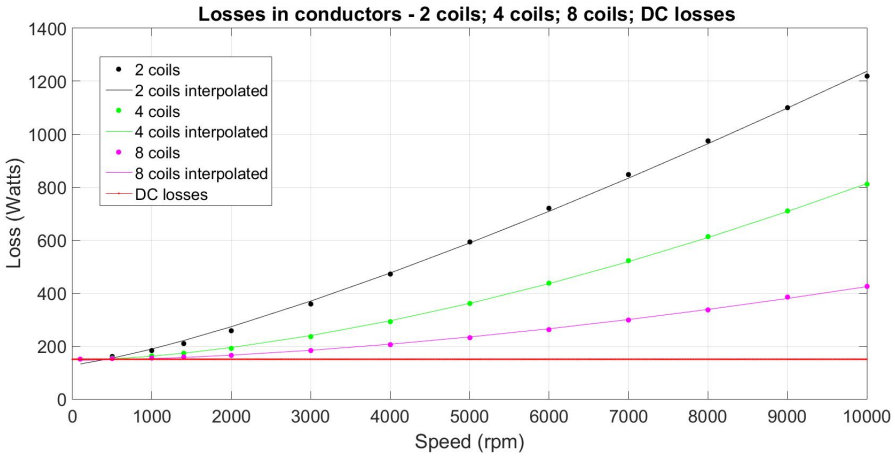

Figure 3-9: Copper losses comparison-2,4,8 conductors in the slot

Transient simulations have been carried out up to 10000 rpm in twelve steps total. Like before, two electric periods have been simulated and results for copper losses are gathered from the Global Results Window. Since the interest is on the steady state losses, the first electric period is not considered due to the initial transient. The losses are represented in the figure 3-9 as colored dots. These dots have then been interpolated using the least squares interpolation method[4]. The constant curve in the figure 3-9 represents the DC losses - where conductors are modeled as "stranded" with uniform current density distribution. As can be seen from the figure 3-9, at low frequencies (less than 500 rpm) the total losses consist mainly out of DC losses. Significant increase in AC losses is noticeable at high operating frequencies. In the case with 2 conductors in slot connected in series, the total copper losses at 10000

[4]Microsoft Excel® solver was used to interpolate the dots with the following function: $ax^2 + bx + c$

rpm reach 1.2 kW (one kilowatt more than DC losses). With 4 conductors per slot, total losses are reduced by more than 400 Watts, still the difference between AC and DC losses is around 660 Watts at this frequency (AC losses are more than 4 times the DC losses). Figure 3-10 shows the ratio between AC losses (4 conductors per slot) and AC losses (2 conductors per slot) for the considered speed range.

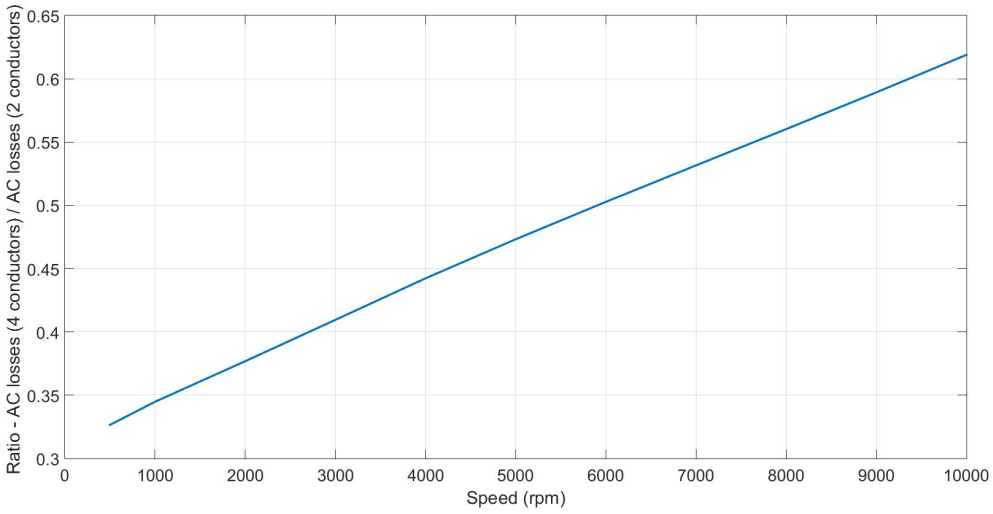

Figure 3-10: Ratio: $\frac{\text{AC losses (4 turns)}}{\text{AC losses(2 turns)}}$

Linear dependency between these two cases can be observed. At maximum operating speed with 4 conductors per slot, losses in the copper are reduced by ∼38% (compared to the case with two conductors per slot).

In the final stage (8 conductor in slot with 1 mm thickness each), the total losses at 10000 rpm add up to 425 Watts (275 Watts belong to AC losses and 150 Watts are DC losses). Comparison to AC losses with 2 conductors per slot is shown in the figure 3-11.

Again, linear dependency between these two cases is noted. In this case, significant reduction in copper losses is present at maximum operating frequency: ∼74% reduction of copper losses compared to the case with two conductors per slot. Further dividing of conductors in the slots is not possible due to conductor thickness and any further ohmic loss reduction would require Litz wire conductors to be implemented.

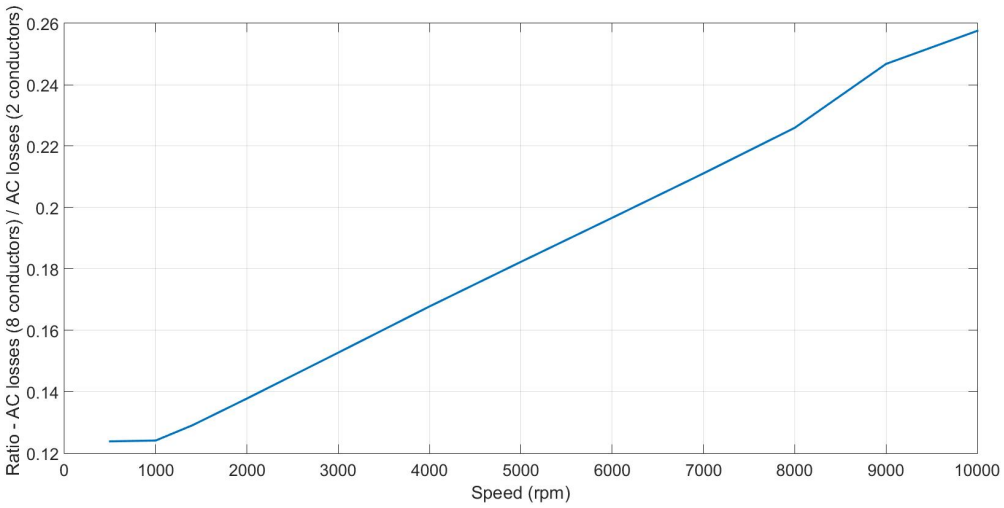

Figure 3-11: Ratio: $\frac{\text{AC losses (8 turns)}}{\text{AC losses(2 turns)}}$

Chapter 4

Thermal Design of the ISG Machine

4.1 Introduction

Along with electromagnetic design, thermal design is an equally important stage in the design process of any electric machine. An insight in heat distribution within the machine is crucial since temperature rise limits the power with which the machine can be constantly loaded[15].

To determine temperature rise and heat flow it is necessary to have an estimation of machine losses (chapter 3) and to know the thermal properties of the materials used in the machine construction. Thermal analysis was carried out in ThermNet® software (Infolytica) where a 2-D model was constructed and 2-D FEA performed. Thermal FEA, like electromagnetic FEA, consists of three main stages:

- Pre-processing;
- Solving;
- Post-processing;

Pre-processing stage is done in MATLAB® where a script is created to construct the geometry, make components, assign materials and boundary conditions and set

solving parameters.

In order to perform thermal analysis, machine components that generate losses have to be defined as heat sources. Based on the results obtained in MagNet® for machine losses, heat source densities (specific losses per volume) are assigned to machine components (stator, wedges and coils). Stator specific losses are calculated by dividing the total core losses (hysteresis and eddy-current losses) by the stator volume. Similar is done for the losses generated in magnetic wedges closing the slots. Specific losses for the coils are obtained by dividing the Joule losses (losses obtained from MagNet® plus the estimated DC end-turn losses) by the coil's volume.

Solving procedure - solving methods and accuracy is identical to the one described for MagNet®.

In the post-processing stage, results such as final temperature levels in machine components, heat flow etc. can be extracted from the Global Results Window.

4.1.1 Modelling the machine geometry in 2-D

The geometry constructed for thermal analysis is shown in the figure 4-1:

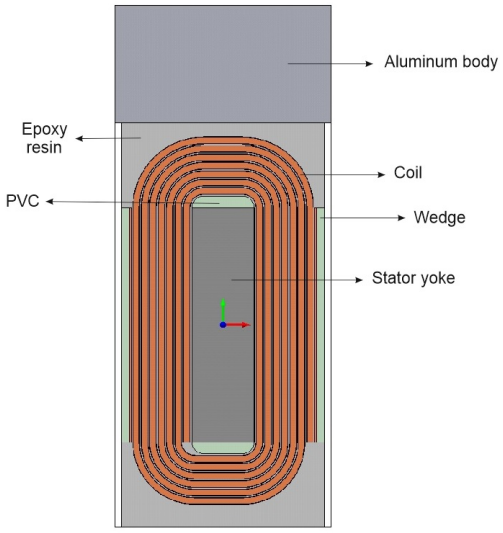

Figure 4-1: Machine geometry constructed for thermal FEA

The 2-D slice presented here differs from the one used for electromagnetic analysis. Only stator yoke section with a full coil (including end-turns) and aluminium body is presented. Both rotors with permanent magnets are not included in the model. Coil is wound in spiral fashion with seven turns equally spaced inside the slots. Aluminium frame (20 mm high) is drawn on top of the model. Both slot tops are closed with magnetic wedges.

Materials which will be used in thermal FEA, and their corresponding thermal conductivities are listed in the table 4.1.

Aluminium is used to construct the machine frame, while copper, Somaloy 500 (magnetic wedges) and listed stator materials were used in electromagnetic analysis described in the previous chapters.

Epoxy resin, Nomex®, Polyimide and PVC are all insulating materials used in the thermal analysis.

Material	*Thermal conductivity(W/°Cm)*
Aluminium	230
Copper	386
Stator material M-250-35A	25
Stator material Vacoflux 48	25
Stator material Vacoflux 50	30-37
Stator materials NO (Cogent)	28
Epoxy resin	0.22
Nomex	0.25
Polyimide	0.35
Polyvinylchloride (PVC)	0.147
Somaloy 500	30

Table 4.1: Materials used for 2-D FEA

Conductor insulation is the most sensitive part in machine insulation since it is directly surrounded with heated copper. Polyimide film is used as conductor insulation for this application (0.06 mm thick layer surrounding the copper). This material can endure constant temperatures up to 220 (°C) and its instantaneous thermal resistance can reach 400 (°C)[15]. This type of conductor insulation is rather expensive compared to commonly used varnishes, but being a very thin insulator it allows for placing more copper inside the slot.

The area inside the slot is filled with epoxy resin in order to mechanically strengthen the winding and protect it from substances such as dirt, moisture and different chemicals.

Coil insulation from the stator iron (slot bottom) and the magnetic wedges (slot top) is done with Nomex® material (0.125 mm layer in the slot bottom and 0.25 mm layer in the slot top). End windings are separated from the stator yoke with a rounded PVC layer with maximum thickness of 2 (mm).

4.1.2 Boundary conditions

Like electromagnetic analysis, thermal analysis requires solving boundary-value problems. It is required to assign the appropriate condition to each of the solution domain's boundaries. Important feature of ThermNet® is that it does not do Computational Fluid Dynamics (CFD) and all the fluid components have to be left out of the solution domain[1]. Boundary conditions offered in ThermNet® are:

- Perfect Insulator (PI);
- Specified Temperature (ST);
- Thermal Environment (TE);
- Even Periodic (EP);
- Convective Gap Link;
- Convective Enclosure Link;
- Thin Layer (TL).

For the analysis performed in this work, PI and ST boundary conditions are used. PI is a default ThermNet® boundary condition which software automatically assigns to the solid component faces. It forbids any heat flow across the boundary.

ST condition is rigorously imposed on the aluminium body component, while other faces are left as perfect insulators.

[1] Air gap components on both sides of the model are assigned with Virtual Air material which is considered as a solid, so the FEA can be successfully performed.

Conclusions

In this thesis, preliminary electromagnetic design stage of an electric machine for an integrated starter/generator application in a hybrid supercar was performed. The double-sided (single slotted stator, double rotor) AFPM topology with surface-mounted permanent magnets was adopted as a most promising topology to meet the strict requirements imposed. Electromagnetic design stage was performed with the help of final element analysis (FEA) in Infolytica's MagNet® software.

The focus of electromagnetic analysis were the torque behaviour and losses minimization. When the machine is operating as a starter motor, very high overload torque (maximum torque to rated torque ratio) needs to be achieved without saturating the machine. 2-D parametric FEA was performed varying the stator current, air gap and wedge gap in order to construct torque-current curves. From these curves it is possible to read the current values required to meet the torque requirements. Results also show the influence of varying the wedge gap (slots are partially closed with magnetic wedges) and air gap parameters on torque behaviour. Combinations of larger wedge gaps (2mm) with smaller air gaps (1mm) offer the highest value of torque with least saturation. However, smaller air gaps are not suitable (bad cooling arrangement for PMs) and can lead to irreversible demagnetization due to the heating of the magnets. Also, considering the high operating frequencies larger air gap offers safer machine operation. Air gap and wedge gap of 2 (mm) both were chosen for further analysis. Further torque behaviour improvement is achieved with testing out various stator materials. Number of thin, non-oriented, high-quality steels were taken into consideration. Parametric 2-D FEA was performed for each of the considered stator materials in order to compare iron losses. Operating point at maximum rotating

speed is the focus of the analysis where losses for reference material (M250-35A) reach 1.2 (kW). VACOFLUX® materials proved as the best solution once again offering considerable loss reduction (∼66% reduction compared to reference material). Re-running 2-D static FEA, results show that cobalt-iron VACOFLUX® materials also offer superior torque behaviour over other materials tested and that required torque levels (starter operation) are achievable. Wide CPSR for generator operation (up to 10000 rpm) cannot be achieved with controlling the stator currents and mechanical flux weakening methods will have to be employed to meet the criteria. Losses in the copper were also extracted from the performed 2-D FEA. DC component of these losses is obtained by modeling the coils as "stranded" (neglecting the skin effect). Not considering the end-windings, DC copper losses add up to 150 (W). A rough estimation of DC losses in end-windings shows that these losses are approximately 50% of the losses inside the slots. To get an estimation of AC component of copper losses, coils have to be modeled as "solid", where current density distribution follows Maxwell's laws. When the machine is running at high frequencies, FEA shows that total copper losses can reach 1.2 (kW) with two conductor turns per slot. To reduce these losses, the number of turns is increased to 4 and 8 turns per slot in order to achieve more uniform current density distribution. Combinations of series and parallel connections were made and significant reduction of AC ohmic losses are achieved - at 10000 (rpm) total losses can be decreased by approximately 74% (with 8 turns per slot copper AC losses are reduced by $\sim 74\%$ compared to the case with 2 turns per slot).

With the help of FEA, machine constants such as phase resistance, synchronous inductance and back-emf were estimated. However, these estimations were made with 2-D analysis where effects of end-windings cannot be included.

Unfortunately, results for thermal analysis - temperature distribution, heat flow etc. were not presented in this work. Certain difficulties in pre-processing stage were encountered which lead to incorrect results. Solution was not found by the time of thesis presentation, and author will try to include these results in further versions of the work.

Future developments

Analyses described in this Master Thesis are part of an initial design stage of the electric machine - they serve just as a feasibility study to roughly check if the required performance is achievable. For that purpose, a fast 2-D FEA was satisfying. However, 3-D FEA has to be used as an absolute predictor of performance.

Future work will include constructing an accurate 3-D machine model (3-D effects such as end-turns will be included) and performing a precise 3-D FEA, both in MagNet® and ThermNet® softwares. 3-D FEA, even though very demanding in time and computing memory, will offer results which would be much closer to the actual machine compared to the ones obtained through 2-D FEA.

Mechanical flux-weakening techniques which are necessary for achieving wide CPSR specified in requirements will have to be further investigated and detailed.

Index

List of Symbols and Abbreviations

A vector magnetic potential

$AFPM$ axial-flux permanent magnet machine

B magnetic flux density

B_m magnetic loading

B_{rem} remanence

$CPSR$ constant power speed range

EMF electromotive force

$E_{0,ph,rms}$ no load, phase back EMF

FEA finite element analysis

FW field weakening

F_x force in x-direction

H magnetic field strength

HEV hybrid electric vehicles

H_c coercivity

ICE internal combustion engine

IM induction machine

IPM interior permanent magnets

ISG integrated starter/generator

L_d d-axis inductance

L_q q-axis inductance

P pole pairs

PM permanent magnet

P_{DC} DC conductor losses

P_{cu} ohmic losses

Q number of slots per pole per phase

$R_{ph,DC}$ phase resistance, DC value

R_{ph} phase resistance

S copper surface

SMC soft magnetic composite

SRM switched reluctance machine

T torque

T_{cog} cogging torque

W_{mc} magnetic co-energy

Z_{base} base impedance

β Steinmetz constant

$l_{q,p.u}$ per unit value of q-axis inductance

λ_{PM} PM flux linkage

λ_{abc} 3-phase flux linkages

λ_d d-axis flux linkage

λ_{qd0} flux linkages, qd0 components

λ_q q-axis flux linkage

ω_e electric speed

ω_m mechanical speed

ρ resistivity

e induced voltage

f frequency

i_d d-axis current

i_q q-axis current

k_{ec} eddy current constant

k_{hy} hysteresis constant

l_{ew} end-winding length

m number of phases

p_{iron} iron losses

r_{avg} average radius

$theta_m$ mechanical angle

k_{fill} fill factor

Bibliography

[1] Nicola Bianchi, Massimo Barcaro, and Silverio Bolognani. *Electromagnetic and Thermal Analysis of Permanent Magnet Synchronous Machines*. InTech, first edition, 2012.

[2] F. Giulii Capponi, G. Borocci, G. De Donato, and F. Carrichi. Flux regulation strategies for hybrid excitation synchronous machines. *IEEE*, 2015.

[3] F. Giulii Capponi, G. De Donato, and F. Carrichi. Recent advances in axial-flux permanent-magnet machine technology. *IEEE*, 2012.

[4] Fabio Giulii Capponi. Lecture notes in dynamic analysis and control of ac machines, 2013.

[5] F. Carrichi, F. Crescimbini, F. Giulii Capponi, and L.Solero. Permanent-magnet, direct-drive, starter/alternator machine with weakened flux linkage for constant-power operation over extremely wide speed range. *IEEE*, 2001.

[6] G. De Donato, F. Giulii Capponi, and F. Carrichi. Influence of magnetic wedges on the load performance of axial flux permanent magnet machines. *IEEE*, 2010.

[7] G. De Donato, F. Giulii Capponi, and F. Carrichi. No-load performance of axial flux permanent magnet machines mounting magnetic wedges. *IEEE*, 2012.

[8] G. De Donato, F. Giulii Capponi, and F. Carrichi. On the use of magnetic wedges in axial flux permanent magnet machines. *IEEE*, 2013.

[9] L. Del Ferraro, F. Carrichi, and F. Giulii Capponi. Analysis and comparison of a speed-dependant and torque-dependant mechanical device for wide constant speed range in afpm starter/alternators. *IEEE*, 2006.

[10] L. Del Ferraro, F. Carrichi, F. Giulii Capponi, and G. De Donato. Axial-flux pm starter/alternator machine with a novel mechanical device for extended flux weakening capabilities. *IEEE*, 2004.

[11] A. E. Fitzgerald, Charles Kingsley Jr., and Stephen D. Umans. *Electric Machinery*. McGraw-Hill, sixth edition, 2003.

[12] Jacek F. Gieras. *Permanent Magnet Motor Technology*. Taylor & Francis Group, LLC, third edition, 2010.

[13] Dr. Duane Hanselman. *Brushless Permanent Magnet Motor Design*. Magna Physics, second edition, 2006.

[14] *Infolytica Help File*.

[15] Juha Pyrhönen, Tapani Jokinen, and Valéria Hrabovcová. *Design Of Rotating Electrical Machines*. John Wiley & Sons, Ltd, first edition, 2008.

[16] Ioan-Adrian Viorel, Loránd Szabó, Lars Löwenstein, and Christian Şteţ. Integrated starter-generator for automotive applications, journal = actaelectrotehnica, year = 2004,.